CHAPTER IV
NOVEL TEMPLATE CONFINEMENT DERIVED FROM POLYBENZOXAZINE-BASED CARBON XEROGELS FOR SYNTHESIS OF ZSM-5 NANOPARTICLES VIA MICROWAVE IRRADIATION

4.1 Abstract

Polybenzoxazine, a new class of phenolic resin, has been successfully synthesized via a facile quasi-solventless method and used as a starting material for producing nano-porous carbon with pore sizes of about 40-200 nm. This porous carbon is prepared via a sol-gel process, using dioxane as a solvent (CXDI) and is used as a hard template confinement to produce crystalline nanosized MFI or ZSM-5 with a molar composition of $10Na_2O:200SiO_2:Al_2O_3:20TPABr:12,600H_2O$ via hydrothermal microwave irradiation technique within 6 h of synthesis time. The XRD patterns show a well-ordered crystalline phase of nanosized ZSM-5. In addition, FTIR result shows the weak absorption band at 550 cm^{-1}, indicating the presence of nanosized ZSM-5. Particle size distribution obtained from dynamic light scattering and TEM images reveal that the crystal size of ZSM-5 synthesized using CXDI as a hard template (ZSM-5-CXDI) is in the range of 27–70 nm. ZSM-5-CXDI also shows large external surface area of 217 m^2/g.

4.2 Introduction

Zeolite Sieve of Molecular porosity – 5, (structure type MFI – mordenite framework inverted), ZSM-5, has been used in various applications especially as a catalyst in organic syntheses, oil refining, environmental management, and petrochemical industry [1-6], because of its outstanding properties. Some of these properties are: shape-selectivity, surface acidity, well-ordered pore network, high thermal stability, and cation-exchange capability. Generally, ZSM-5 is a microporous, aluminosilicate material, having crystal size in a micrometer range. These properties could influence the catalytic performance for synthesis of large molecules due to a limitation of mass transfer [5, 7]. Therefore, many researchers have been interested in synthesizing mesoporous ZSM-5, for the improvement of catalytic properties using carbon aerogel [8-10], polymer [11-12], surfactant [13-14] as a template.

Another way to improve the catalytic performance of ZSM-5 is decreasing the crystal size to nanoscale to enable more active sites, resulting in the increased catalytic efficiency [2, 15]. Using this ZSM-5 nanocatalyst, Serrano *et al.* [2] studied the epoxidation rearrangement reactions and found that nanocrystalline ZSM-5 with the crystal size in the range of 20-50 nm showed higher epoxide conversion than microcrystalline ZSM-5 with the crystal size of 5 μm. Furthermore, ZSM-5 nanoparticles were also used as a membrane to effectively separate butane isomers at high temperature [16].

Mesoporous ZSM-5 and ZSM-5 nanoparticles were generally synthesized by using resorcinol-formaldehyde (RF)-based carbon aerogel (or carbon xerogel) as a templating confinement to control the size and the pores of the ZSM-5 crystals [8-10, 17-18]. In this work, we proposed a novel hard template derived from polybenzoxazine. Polybenzoxazine (PBZ) was chosen as a starting material to produce carbon aerogel/xerogel since it has many prominent advantages including ring-opening polymerization without added initiators or catalyst, no release of volatiles during polymerization, near-zero volumetric change upon polymerization, and low water adsorption. Of particular interest in the current project is the excellent molecular design flexibility of the benzoxazine chemistry by varying types of amines

and phenols [19-28] which could tailor the pore structure of PBZ-based organic xerogel and carbon xerogel after carbonization [29-31]. PBZ is easily synthesized by the Mannich condensation reaction of phenol, formaldehyde, and amine via a quasi-solventless route adapted from the solventless method, proposed by Ishida [32]. PBZ is a cross-linked polymer with additional extensive hydrogen bonded networks which can withstand pore collapse without the need of supercritical CO_2 drying process. The shorter preparation time with fewer steps is required when PBZ is used as a precursor for carbon aerogel/xerogel preparation.

A homogeneous orthorhombic MFI zeolite has been successfully synthesized using silatrane, a novel organosilicate material, as a Si source via sol-gel process at 150 °C microwave temperature for 20 h by Phiriyawirut *et al.* who found that the formation rate of MFI depended on OH^- concentration, Na^+ concentration, and organic template concentration. Moreover, they also found that the reaction temperature was related to both aging and heating time. The longer aging time is more important for obtaining high crystallinity MFI than the heating time [33].

In this work, we used PBZ-based carbon xerogels as a novel templating confinement to produce ZSM-5 nanoparticles via microwave irradiation. The effects of the resulting hard carbon template on the microstructure of ZSM-5 were also investigated.

4.3 Experimental

4.3.1 Materials

Main-chain type benzoxazine polymer (MCBP) with benzoxazine group as part of the chemical repeat unit was used as a precursor for carbon xerogels. The MCBP was synthesized from bisphenol-A (BA, 97%, Aldrich), triethylenetetramine (TETA, FACAI Group Limited, Thailand) and formaldehyde (37% w/w, Merck Limited, Germany) using dioxane and dimethylformamide (DMF) as solvents and the polymer is hereinafter abbreviated as MCBP(BA-teta). Dioxane and DMF were purchased from Labscan Asia Co., Ltd., Thailand (analytical grade). All chemicals were used without further purification.

For synthesis of nanosized ZSM-5, tetraethylorthosilicate (TEOS, >98%, Fluka), tetrapropylammonium bromide (TPABr, >98%, Fluka), sodium hydroxide pellets (NaOH, >99%, Labscan Asia Co., Ltd., Thailand), and aluminum-tri-isopropoxide ($Al(iPrO)_3$, 97% , Aldrich) were used without purification.

4.3.2 Synthesis of polybenzoxazine-based carbon xerogels

4.3.2.1 Synthesis of organic gels

The quasi-solventless method adapted from the solventless method proposed by Ishida [32] was used to synthesize benzoxazine prepolymer with a mole ratio of 1:1:4 bisphenol-A:TETA:formaldehyde. Unlike the conventional method which took 5 hours, the reaction was completed within an hour [24]. Bisphenol-A and formaldehyde were separately dissolved in dioxane and DMF and magnetically stirred for 20 min before slowly dropping TETA into the mixture. The mixture was continuously stirred in an ice bath for 1 h until transparent yellow benzoxazine prepolymer was obtained. The prepolymer was then put in a closed system and left for one day, followed by heating at 80 °C for 2 days in an oil bath to let the gel set. After that, white opaque benzoxazine gel was immersed in acetone for 3 days before solvent removal by ambient pressure drying. The resulting organogel was then cured at 160 ° C and 180 °C for 3 h at each temperature, and 200 °C for 1 h to obtain the fully-cured polybenzoxazine with high porosity [30]. *Note:* The concentration of benzoxazine prepolymer was kept at 45% w/w. Polybenzoxazine-based carbon xerogels using dioxane and DMF as solvents were abbreviated as CXDI and CXDM, respectively.

4.3.2.2 Pyrolysis process

Fully-cured polybenzoxazine xerogels were pyrolyzed under nitrogen flow of 600 cm^3/min, using following step pyrolysis: 30–250 °C for 1 h, 250–600 °C for 5 h, 600–800 °C for 1 h and hold at 800 °C for 2 h, followed by cooling to room temperature under nitrogen atmosphere. All processes are summarized in Scheme 4.1.

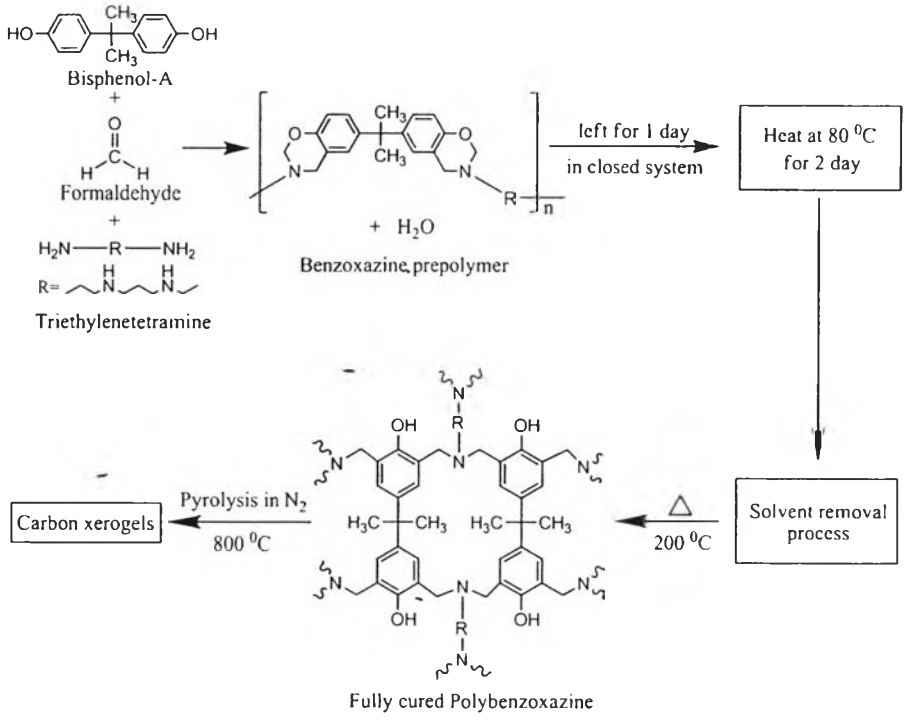

Scheme 4.1 Synthesis diagram of PBZ-based carbon xerogels.

4.3.3 Synthesis of ZSM-5 nanoparticles

The mixture of 10 Na_2O:200 SiO_2:Al_2O_3:20 TPABr:12,600 H_2O [17, 34] was prepared by mixing TEOS and $Al(iPrO)_3$, NaOH, and TPABr. Then, 1 g of PBZ-based carbon xerogels was added and evacuated until no bubble was observed [17] and aged for 5 h before heating in a microwave (MILESTONE, ETHOS SEL, Type ETHOS Plus 2, Operating power of 600 W) at 150 °C for 6 h. The crystallization reaction took place in a closed vessel during microwave irradiation. After the reaction, the mixture was cooled to room temperature and filtered. The precipitate was washed with distilled water until pH became neutral (≅7) and dried at 110 °C for 2 days to remove water prior to calcination at 550 °C for 18 h with a heating rate of 1 °C/min to remove all organics and carbon xerogels template. Finally, white powder of ZSM-5 was obtained.

4.3.4 Characterization

The morphology and microstructure of carbon xerogels and ZSM-5 were observed by using field emission scanning electron microscope (FE-SEM, Hitachi/S-4800 model) and transmission electron microscope (TEM, JEOL 2010F). X-ray diffractometer (Bruker AXS, Germany Model D8 Advance) with CuK_α radiation, a generator voltage of 40 kV, and current of 30 mA, was used to observe the crystallinity of ZSM-5. The scan speed of 1° (2θ)/min with a scan step of 0.01° (2θ) was used to continuously run between 5° and 50° (2θ) range. The broad amorphous (located at 2θ =17°–29°) and crystalline contributions were used to calculate the relative fraction of crystalline phase of the sample, using the ratio of peak height (Z/T), where Z represents the peak height of the {501} crystalline plane contribution of ZSM-5 and T represents the total peak height, including the amorphous height, at the same angle, respectively [17]. The particle size distribution of ZSM-5 nanoparticles was measured by dynamic light scattering technique (Malvern Zetasizer Nano Series, Malvern Instruments Ltd.). The nitrogen adsorption-desorption measurement apparatus was used to determine the porous structure of carbon xerogels and ZSM-5, using Quantachome-Autosorp1-MP. The samples were degassed at 300 °C for 15 h before each measurement. The microporous properties and external surface area were calculated from the t-plot method [35]. The mesoporous properties were analyzed by the BJH method [36-37], and the specific surface area was determined by the BET theory. FT-IR spectra and ^{1}H NMR spectra were recorded on Thermo Nicolet Nexus 670 model and Varian Mercury 300 (300 MHz) apparatus, respectively.

4.4 Results and Discussion

4.4.1 Confirmation of polybenzoxazine structure

The chemical structure of the benzoxazine, main-chain type benzoxazine polymer derived from bisphenol A and teta, hereinafter abbreviated as

MCBP(BA-teta), was confirmed by FTIR and ^{1}H-NMR. The intensity of trisubstituted benzene ring at 1504 cm^{-1} and out-of-plane bending vibrations of the benzene ring at 936 cm^{-1} confirmed that the main-chain type benzoxazine precursor was successfully obtained [38]. After the precursors were fully cross-linked, the intensities of these two bands significantly decreased, indicating that the ring-opening of oxazine ring took place. The ^{1}H-NMR result indicates the oxazine ring formation, as can be seen from the characteristic peaks at 4.82 ppm (O-CH_2-N) and 3.94 ppm (Ar-CH_2-N), representing the protons of methylene bridge in oxazine ring. The peak at 1.55 ppm corresponds to the protons of methyl groups in bisphenol-A. Moreover, the proton resonance belonging to aliphatic amine is found at 2.86 ppm and the resonance at 3.70 ppm represents the protons of -CH_2- of the opened oxazine ring, indicating that MCBP(BA-teta) was in a partially-cured state. All data from FTIR and ^{1}H-NMR are consistent to the results of Katanyoota et al. [30].

4.4.2 Microstructure of PBZ-based carbon xerogels

Generally, RF-based carbon aerogels are used as a templating confinement to produce mesoporous ZSM-5. These carbon materials have the pore diameter in the range of 10–30 nm [8-10]. In this work, PBZ-based carbon xerogels, CXDI and CXDM, were prepared using dioxane and DMF as solvents, respectively, via ambient pressure drying. The physical properties of these carbon xerogels are given in Table 4.1. The specific surface area of both samples are around 311–312 m^2/g. Although both samples provided almost the same specific surface area, the mesopore surface area and mesopore volume of CXDI are higher, around 35 m^2/g, and 0.27 cc/g, respectively, than those of CXDM. The average mesopore diameter of CXDI and CXDM is 3.70 and 3.66 nm, respectively, whereas the average pore diameter is 5.40 and 2.67 nm, respectively. CXDI has an average pore diameter larger than an average mesopore diameter, indicating that macropores are present in CXDI as confirmed by the N_2 adsorption isotherm in Figure 4.1, in which the adsorption branch did not reach the plateau region at the high relative pressure.

Table 4.1 Pore structure of PBZ-based carbon xerogels using DMF and dioxane as solvents via ambient pressure drying at concentration of 45% w/w

Sample	S_{BET} (m^2/g)	S_{meso} (m^2/g)	V_{micro} (cm^3/g)	V_{meso} (cm^3/g)	V_{total} (cm^3/g)	APD_{micro} (nm)	APD_{meso} (nm)	APD (nm)
CXDM*	312	10	0.14	0.05	0.19	1.10	3.66	2.67
CXDI	311	35	0.13	0.27	0.40	1.30	3.70	5.40

Notes : *: ref 19; S_{BET}: BET surface area; S_{meso}: mesopore surface area; V_{micro}: micropore volume; V_{meso}: mesopore volume; V_{total}: total pore volume; APD_{micro}: average micropore diameter; APD_{meso}: average mesopore diameter; APD: average pore diameter

On the other hand, for CXDM, an average pore diameter is smaller than an average mesopore diameter implying that a large amount of micropores is present in CXDM as shown in Table 4.1. However, CXDM still contains a small amount of macropores as confirmed by the N_2 adsorption isotherm (Figure 4.1). At the high relative pressure, the adsorption branch of CXDM does not reach the plateau region as well as that of CXDI but the amount of uptake is different.

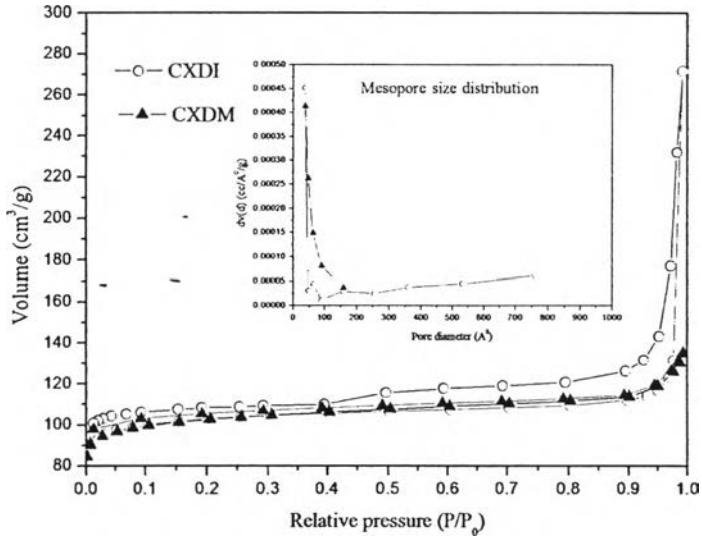

Figure 4.1 Adsorption isotherms of PBZ-based carbon xerogels prepared from 45% w/w of benzoxazine precursor using (▲) DMF (CXDM) [19] and (○) Dioxane (CXDI) as solvents via ambient pressure drying.

Figure 4.2a illustrates the morphology of CXDM, showing very large opened network structure (500 nm-2 μm) [19]. Illustrated in Figure 4.2b are the SEM micrograph and TEM image (inset) of CXDI which shows that this porous carbon also contains macropores (>50 nm) in the structure. However, large macropores could not be detected by N_2 adsorption due to the limitation of the Kelvin equation [39-41] since CXDI mostly contain mesopores and macropores (40-200 nm). According to the IUPAC classification, it was found that the adsorption isotherms of both samples are a combination of the standard isotherm between type IIb isotherm with a H3 hysteresis loop and type Ic isotherm with low relative pressure hysteresis loop due to a capillary condensation, in which type Ic represents microporous adsorbent containing mesopores and type IIb represents macroporous adsorbent [40-42]. The combination of micropores, mesopores, and macroporores in both samples is the cause of a deviation from the ideal isotherm and low relative pressure hysteresis loop, as described by Lorjai et al. [29] who prepared porous carbon from bisphenol-A and aniline based polybenzoxazine. Higher amount of adsorption volume and lager hysteresis loop at high relative pressure of CXDI are the evidence confirming the presence of larger mesopore of CXDI, as shown in Figure 4.1, than CXDM.

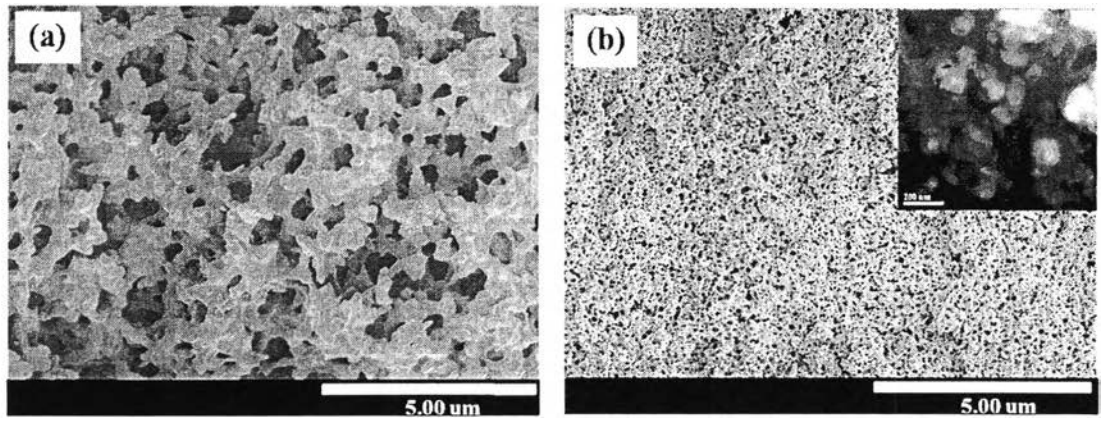

Figure 4.2 Pore structure of PBZ-based carbon xerogels prepared from 45% w/w of benzoxazine precursor using (a) DMF (CXDM) [19] and (b) Dioxane (CXDI) as solvents via ambient pressure drying.

One of the important parameters affecting the pore structure is the difference in the solubility parameter of the solvents used since the formation of polymer cluster during phase separation varies with different solvents. The time corresponding sol-gel transition was related to the rate of cluster growth as indicated by the gelation time. During the sol-gel process, the molecular weight of benzoxazine precursor in the solution was increased relating to the time, resulting in the formation of benzoxazine clusters due to the phase separation phenomena. Finally, the macroscopic gelation point was obtained by inter-connected benzoxazine clusters, as indicated by the gelation time, resulting in the creation of pores after solvent removal process.

By using DMF as a solvent, CXDM showed shorter gelation time (3 h) indicating that when benzoxazine precursors polymerized into larger molecules in DMF, the resulting polybenzoxazines preferred to separate from DMF due to the immiscibility of polybenzoxazine in DMF. The opened network structure was created by large polybenzoxazine clusters after the solvent removal process.

On the contrary, by using dioxane as solvent, CXDI showed a longer gelation time (120 h) and the pore size was in the range of meso-macropore which was smaller than the opened network structure of CXDM. This is in part related to the tendency of oxazine ring opening. Oxazine rings tend to open in solvents with large dielectric constants such as hydrophilic solvents, whereas in a solvent, such as dioxane with low dielectric constant, it is more difficult to open. Thus, the formation of extended molecular structure is easier to achieve in DMF than in dioxane. The phase separation took place after much larger crosslinked polymer molecules were formed. Then, small clusters of polybenzoxazine and meso-macropore were obtained after the removal of solvent (Figure 4.2b). Scheme 4.2 shows the formation of benzoxazine wet gel during the sol-gel process.

In 2006, Ozaki *et al.* [17] found that the percentage of inorganic content (ZSM-5 nanoparticles) increased with the increase of mesoporous surface area of RF-based carbon aerogels. Thus, some macropores contained in mesoporous carbon might have a significant effect on the synthesis of mesoporous ZSM-5 and ZSM-5 nanoparticles due to high accessibility of reaction mixture into the pores of carbon [8-10, 17, 43-44]. As a result, carbon xerogels derived from using dioxane as

a solvent, CXDI, could be suitable as a template confinement due to their larger mesopore and macropore volume.

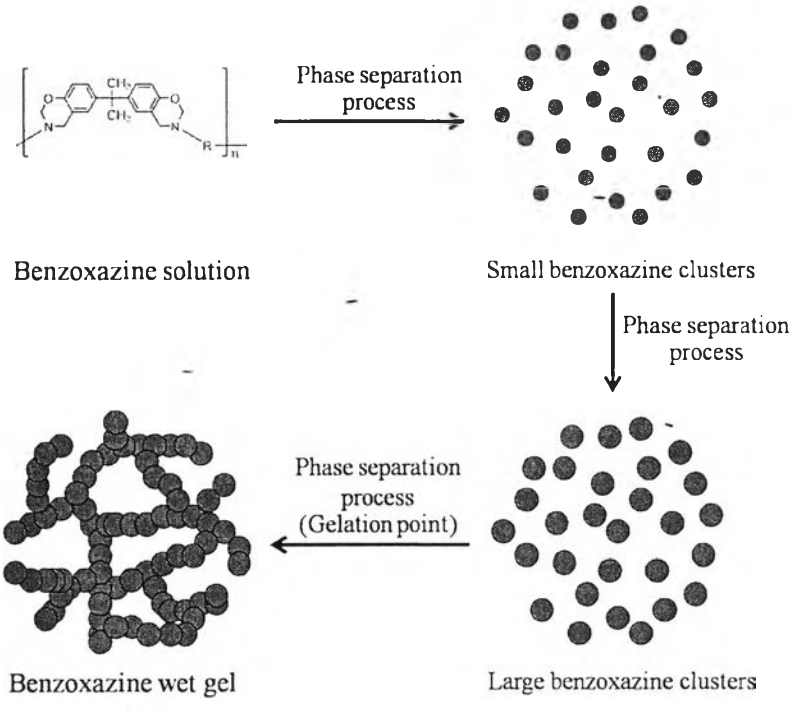

Scheme 4.2 Formation of benzoxazine wet gel during the sol-gel process.

4.4.3 Synthesis of nanosized ZSM-5 in the presence of PBZ-based carbon xerogels

Polybenzoxazine-based carbon xerogels were used as the hard template for the synthesis of ZSM-5 nanoparticles, abbreviated as ZSM-5-CXDI and ZSM-5-CXDM for ZSM-5 synthesized using CXDI and CXDM as the hard template, respectively. The XRD diffractograms in Figure 4.3 illustrate the patterns of ZSM-5 (2θ = 7.89°, 8.82°, and 23.23°) successfully synthesized in the presence of CXDM and CXDI hard template. The diffractrogram peaks of ZSM-5-CXDI (Figure 4.3a) are slightly broader and apparently show the lowest intensity of crystalline peaks, comparing to those of ZSM-5-CXDM and ZSM-5 reference, implying the presence of nanosized ZSM-5 [15, 44-47]. The relative fractions of crystalline phase of ZSM-5-CXDI and ZSM-5-CXDM were 0.88 and 0.94, respectively.

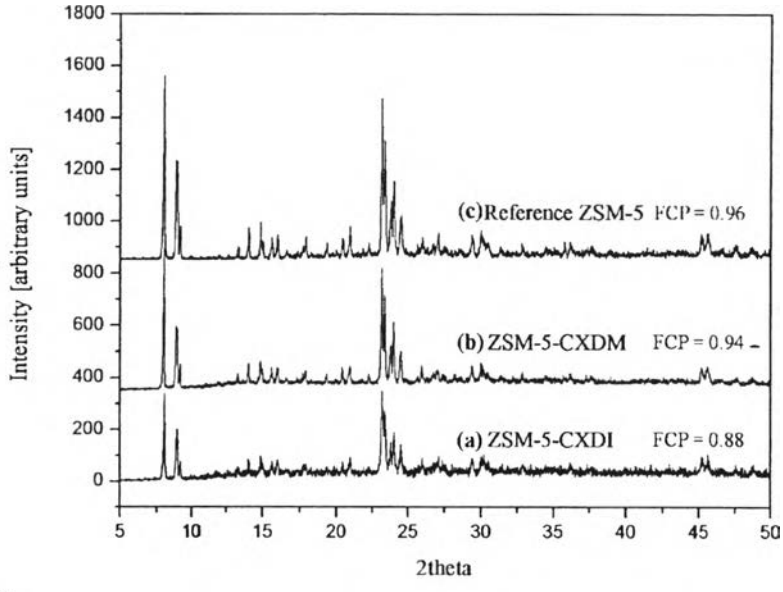

Figure 4.3 XRD patterns of ZSM-5 formed at 150 °C for 6 h after 5 h aging time using (a) CXDI, (b) CXDM as hard template, (c) reference ZSM-5 without hard template carbon, FCP = fraction of crystalline phase.

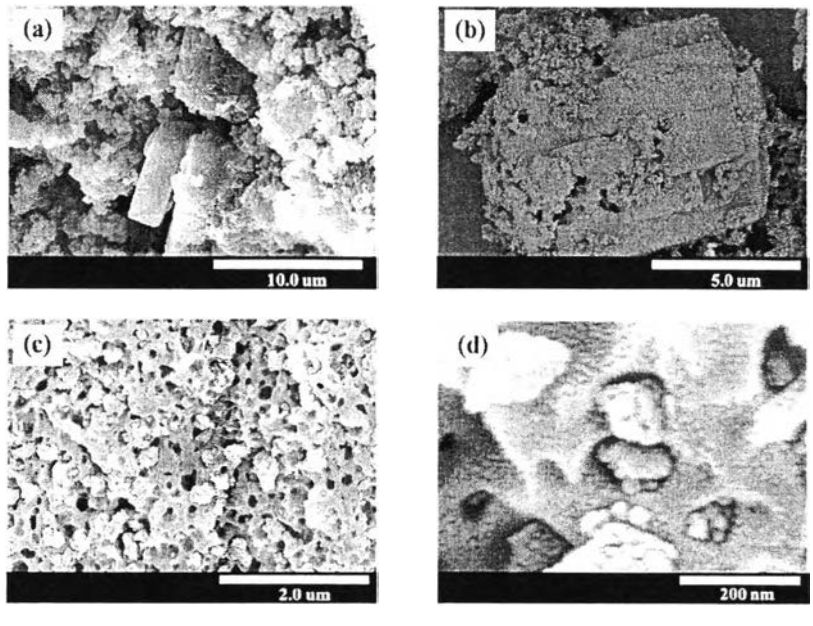

Figure 4.4 SEM micrographs of ZSM-5 formed at 150 °C for 6 h after 5 h aging time; (a) microsized ZSM-5 formed in the opened structure of CXDM, (b) microsized ZSM-5 with monolithic pore after calcinations, (c)-(d) nanosized ZSM-5 formed in the pores of CXDI.

The SEM micrographs in Figures 4.4c and d reveal that nanosized ZSM-5 zeolites were achieved by using the CXDI hard template because the optimum pore size of CXDI was in the range of nanoscale to confine the ZSM-5 particles as shown in Figure 4.2b, generating nanosized ZSM-5 whereas most of the pores of CXDM were opened structure with a micrometer-size scale as shown in Figure 4.2a, resulting in the micrometer-sized ZSM-5 formed in the opened structure of CXDM as shown in Figure 4.4a. After calcination, the micrometer-sized ZSM-5 with monolithic pores were obtained, as a result of the growth of ZSM-5 crystal partially or entirely encapsulated in large carbon particles, as represented in Figure 4.4b.

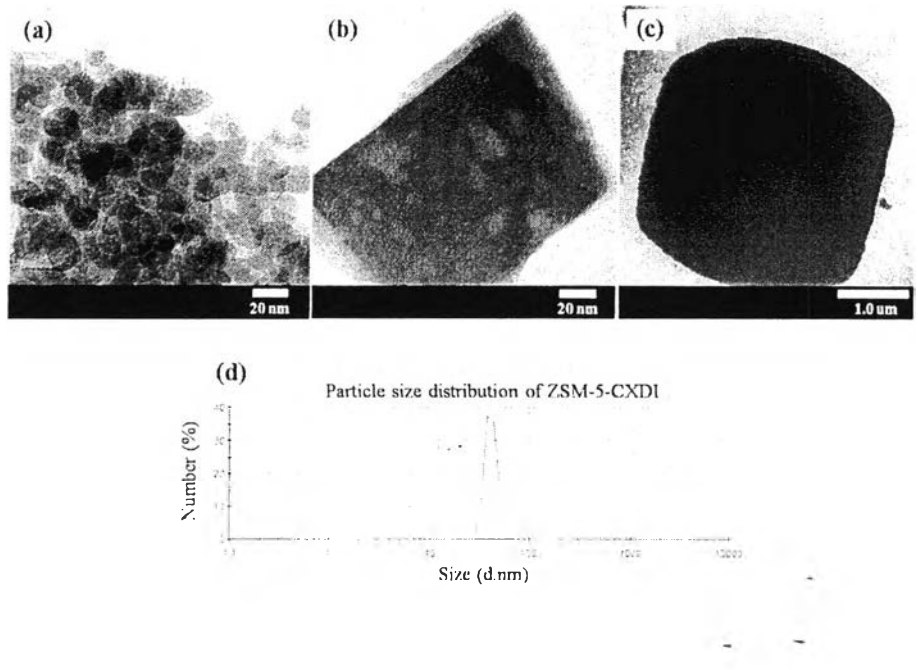

Figure 4.5 TEM images of ZSM-5 formed at 150 °C for 6 h after 5 h aging time, using carbon xerogels as hard template; (a)-(b) ZSM-5-CXDI (c) ZSM-5-CXDM (d) Particle size distribution of ZSM-5-CXDI obtained from dynamic light scattering.

TEM images in Figures 4.5a-c and SEM micrographs in Figure 4.4 were used to confirm the size of ZSM-5 produced by CXDI and CXDM in which the particle size of each ZSM-5 was identical with the pore size of its own carbon template as supported by pore structure of carbon xerogel in Figure 4.2. According to the TEM images and particle size distribution obtained from dynamic light scattering

(Figure 4.5a, b and d), the crystal size of ZSM-5-CXDI is in the range of 27–70 nm, and its mean particle size is around 41.2 nm which corresponds to the pore size of CXDI in Figure 4.2b. However, in Figures 4.4c-d and 4.5a, an agglomeration of ZSM-5 nanoparticles with some inter-growths between small crystals is observed. The crystal size of ZSM-5-CXDM is mostly in the range of 3–10 μm (Figures 4.4b and 4.5c), which is identical to the size of the opened structure of CXDM (Figures 4.4a and 4.2a). The precursor of ZSM-5 was in the liquid state which could penetrate into pores of CXDM and CXDI after evacuation. During the crystallization reaction, the crystal size of the obtained ZSM-5 was confined by the pore size of carbon xerogels templates. Therefore, the size of ZSM-5 crystal was identical with the pore size of its own carbon xerogel template. According to the obtained results of ZSM-5, it was shown that the pore structure of PBZ-based carbon xerogels had significant effect on the size of as-synthesized ZSM-5. By varying the types of solvents, different pore structures of carbon xerogels were easily achieved. Figure 4.6 reveals the crystal lattice of ZSM-5-CXDI of 0.3–0.5 nm which is in good agreement with Cheng *et al.*'s work in which nanosized ZSM-5 with the crystal lattice of 0.3 nm was produced in the absence of organic template via hydrothermal treatment at temperature of 180 °C for 24 h [48].

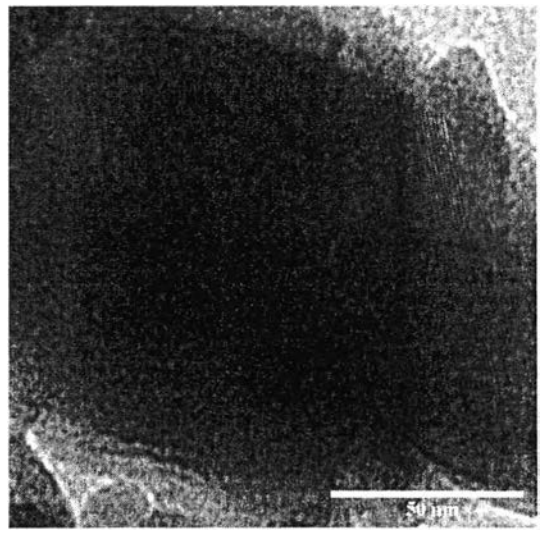

Figure 4.6 Crystal lattice of nanosized ZSM-5 formed at 150 °C for 6 h after 5 h aging time, using CXDI as hard template.

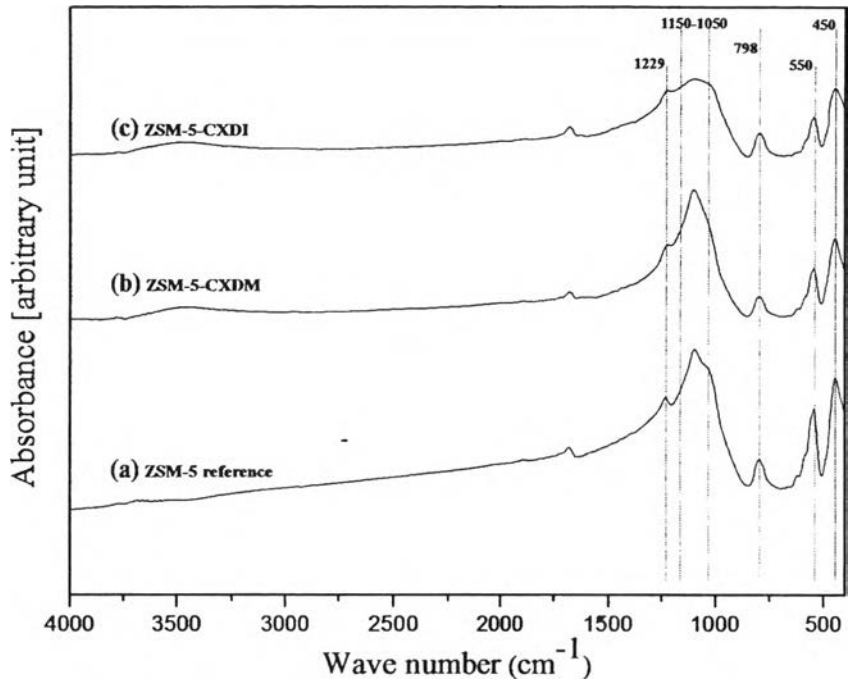

Figure 4.7 FTIR spectra of ZSM-5 formed at 150 °C for 6 h after 5 h aging time; (a) ZSM-5 reference (b) ZSM-5-CXDM (c) ZSM-5-CXDI.

FTIR spectra are also used to confirm the presence of nanosized ZSM-5. From Figure 4.7, all samples show typical absorption peaks of highly siliceous material at the wavenumber of 1229 cm^{-1} (external asymmetric stretch vibration of the T-O bond), 1150–1050 cm^{-1} (internal asymmetric stretch of T-O), 798 cm^{-1} (external symmetric stretch of T-O), and 450 cm^{-1} (T-O bend) [49-54]. In particular, the absorption peak at 550 cm^{-1} (dyad five-member ring) is the characteristic peak of ZSM-5, representing the vibration of framework formed by tetrahedral SiO_4 and AlO_4 unit [49, 55]. The peak intensity ratio of 550 cm^{-1} and 450 cm^{-1} (I_{550}/I_{450}), or the so-called optical density ratio, can approximately estimate the relative degree of crystallinity [43, 56-58]. The optical density ratio of all samples is 0.78, 0.75, and 0.68 for the ZSM-5 reference, ZSM-5-CXDM, and ZSM-5-CXDI, respectively. Furthermore, the obtained optical density ratio of 0.78 of the ZSM-5 reference is almost the same as that of pure pentasil sample in the literature, which is 0.80 [58]. The weak absorption bands at 550 and 450 cm^{-1} of ZSM-5-CXDI compared to that of the ZSM-5 reference (Figure 4.7c) are evidence of the nanosized ZSM-5 formation

of the less-ordered frame structure, which is highly consistent with the results reported in the literature that the nanosized ZSM-5 showed weak framework vibrations at 550 and 450 cm^{-1}, and lower intensities of XRD diffractograms than those of the micrometer-sized ZSM-5 [15, 44-47]. The result shows that the less-ordered frame structure was observed with decreased crystal size, which is strongly supported by the XRD data, TEM images, and FTIR spectra. All data suggest that CXDI is an appropriate template to produce ZSM-5 in nanoscale whereas CXDM produces mostly ZSM-5 in the micrometer-scale.

4.4.4 Pore structure of nanosized ZSM-5

The nitrogen adsorption isotherms of all samples are shown in Figure 4.8. According to the classification by IUPAC on adsorption isotherms, ZSM-5-CXDI and ZSM-5-CXDM basically belong to the type IV isotherm with H1 hysteresis loop, representing the properties of mesoporous materials [40-41]. The hysteresis loop of H1 also suggests that ZSM-5-CXDI and ZSM-5-CXDM have narrow distribution of uniform pores [41] whereas the ZSM-5 reference exhibits type I isotherm, corresponding to the properties of microporous material [40-41]. All samples have high uptake at low relative pressure, representing the adsorption by the micropores, while the additional uptakes at a high relative pressure representing the adsorption by the mesopores and macropores. Mesopore size distribution of ZSM-5-CXDI and ZSM-5-CXDM is around 3–50 nm with the average mesopore size around 24.95 nm for ZSM-5-CXDI and 3.57 nm for ZSM-5-CXDM. The highest BET surface area of 356 m^2/g, mesopore volume of 0.41 cc/g, and mesopore surface area of 68 m^2/g are also obtained from ZSM-5-CXDI. From Figure 4.5d, the crystal size distribution of ZSM-5-CXDI is around 27–70 nm. Figure 4.5b shows the crystal size of ZSM-5-CXDI, containing some pores inside the structure. Moreover, there is an indication that during the crystal inter-growth inside the carbon, ZSM-5 crystals encapsulated some parts of carbon, generating the intra-pore size of 10–30 nm after carbon removal. However, for the ZSM-5-CXDI with small crystal size, no intra-pores in the crystal are observed as shown in Figure 4.5a, because the crystals were too small to encapsulate carbon. As a result, the small crystals of ZSM-5-CXDI

exhibited the microporous properties similar to those of the ZSM-5 reference. In addition, small crystals of ZSM-5-CXDI exhibited the mesoporous properties due to the inter-pore between nanocrystals generated by the aggregation of the nanosized crystals, as shown in Figure 4.5a [2, 15, 45].

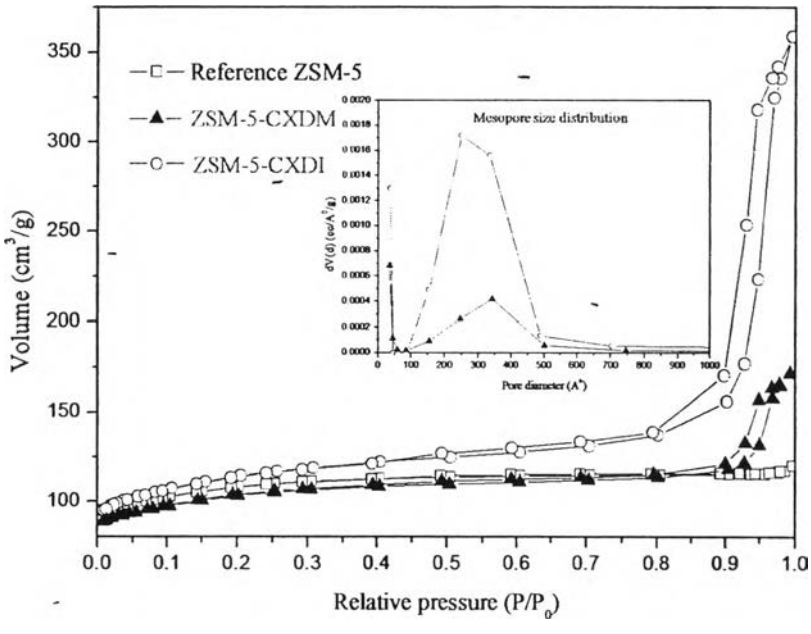

Figure 4.8 Adsorption isotherms of ZSM-5 formed at 150 °C for 6 h after 5 h aging time; (▲) ZSM-5-CXDM (○) ZSM-5-CXDI (□) Reference ZSM-5.

By using CXDI as a hard template, the well-defined ZSM-5-CXDI consisting of two types of nanoparticles; large nanosized ZSM-5 with intra-pore and small nanosized ZSM-5 without intra-pore were obtained. Moreover, the mesopore of ZSM-5-CXDI could be divided into two types; the inter-mesopores generated by aggregation of small nanosized ZSM-5 and the intra-mesopores generated inside large nanosized ZSM-5. In addition, there was no mesopore observed in the large crystals of ZSM-5-CXDM (Figure 4.5c). The large amount of micropore volume and TEM images of ZSM-5-CXDM provide evidence to confirm that most of ZSM-5-CXDM exhibited traditional micropores similar to the ZSM-5 reference. However, ZSM-5-CXDM still has a small amount of mesopore which can be described in terms of crystallization of ZSM-5 inside the carbon templates. Although a large amount of

micropore volume was found in CXDM, CXDM still contained a small amount of mesopore as well. Therefore, there are chances for ZSM-5 precursors to penetrate and crystallize inside the carbon substrate. So, small nanosized ZSM-5 can be generated. Hence, mesopore could be generated from the aggregation of small nanosized ZSM-5 (inter-mesopores) or carbon encapsulation of ZSM-5 showing partial characteristic isotherm of mesoporous material in Figure 4.8.

Table 4.2 Pore structure of ZSM-5 formed at 150 °C for 6 h after 5 h of aging time

Sample	S_{BET} (m^2/g)	S_{meso} (m^2/g)	V_{micro} (cm^3/g)	V_{meso} (cm^3/g)	V_{total} (cm^3/g)	APD_{micro} (nm)	APD_{meso} (nm)	APD (nm)
Ref. ZSM-5	334	6	0.15	0.02	0.17	0.50	3.57	2.22
ZSM-5-CXDM	320	20	0.13	0.11	0.24	0.50	3.57	3.32
ZSM-5-CXDI	356	68	0.07	0.41	0.48	0.50	24.95	6.23

Notes: S_{BET}: BET surface area; S_{meso}: mesopore surface area; V_{micro}: micropore volume; V_{meso}: mesopore volume; V_{total}: total pore volume; APD_{micro}: average micropore diameter; APD_{meso}: average mesopore diameter; APD: average pore diameter

Moreover, the small amount of mesopore volume of ZSM-5-CXDM (~0.11 cc/g) was lower than that of ZSM-5-CXDI (0.41 cc/g). However, in the case of intra-mesopore generated by carbon encapsulation, the formation of this type was totally random and not reproducible. Although the reason for the mesoporous properties of ZSM-5-CXDM was the same as those of ZSM-5-CXDI, the pore structure of ZSM-5-CXDI and ZSM-5-CXDM was different due to the difference in pore structure of its own carbon template to confine the size of ZSM-5, resulting in difference in size and pore structure of the obtained ZSM-5.

All results suggest that difference in pore structure of PBZ-based carbon xerogels plays an important role in confining the size of ZSM-5 nanoparticles and also their porous properties. By using dioxane and DMF as solvents, the meso-macro pore and the opened network structure were achieved from CXDI and CXDM, respectively. ZSM-5 nanoparticles with particle size of 27-70 nm were achieved by using CXDI as hard template because CXDI had the optimum pore size in the range

of nanoscale to confine the crystal size of ZSM-5. Whereas, ZSM-5-CXDM with the particle size of 3–10 μm was confined by CXDM corresponding to the pore size of its carbon hard template. The pore structure of the synthesized ZSM-5 is summarized in Table 4.2. It was found that ZSM-5-CXDI shows a large mesopore volume with mesopore diameter of 24.95 nm and large external surface area. These properties could influence the catalytic performance for synthesis of large molecules such as good mass transfer of reactants and products, and more active sites on the surface to increase catalytic efficiency. Many research groups synthesized ZSM-5 nanoparticles without intra-mesopores [2, 15, 17, 44-45]. However, in 2008, Fang *et al.* [43] synthesized mesoporous MFI single crystal using ambient drying RF-based carbon aerogels as a secondary template via hydrothermal treatment at temperature of 170 °C for 48 h and found that the intra-crystal mesopores of MFI zeolites could be achieved by varying the catalyst concentrations during RF synthesis.

4.5 Conclusions

By taking advantage of molecular design flexibility, novel carbon xerogels derived from PBZ with tailorable pore structure were successfully synthesized via a facile synthesis process and used as a template confinement. Moreover, by using PBZ as a precursor, the preparation of carbon xerogels was more time efficient when compared with those prepared from RF as previously reported. When dioxane was used as a solvent, CXDI showed the highest mesopore volume and mesopore surface area. In addition, some mesopores and macropores contained inside the structure of CXDI, with pore diameters of 40-200 nm, could facilitate the precursors of ZSM-5 to penetrate inside porous carbon and crystallize as nanosized ZSM-5. Using this novel template confinement as a hard template, CXDI template, highly crystalline nanosized ZSM-5 was successfully synthesized at 150 °C for 6 h with 5 h aging time via microwave irradiation. The resulting ZSM-5-CXDI with crystal sizes of 27-70 nm exhibited the mesoporous properties and high external surface area. The crystal size of ZSM-5-CXDI was identical with the pore size of the original CXDI template. According to the obtained results mentioned above, the CXDI template was an

appropriate template to produce ZSM-5 nanoparticles. The morphology of the carbon xerogels played an important role in the properties of the synthesized ZSM-5. Hence, the properties of synthesized ZSM-5 could be easily tailored by changing carbon xerogel templates.

4.6 Acknowledgements

This work has been financially supported by the National Nanotechnology Center (NANOTEC), and the National Center of Excellence for Petroleum, Petrochemicals, and Advanced Materials, Chulalongkorn University. In addition, the authors would like to thank Prof. Suwabun Chirachanchai for DLS apparatus, Mr. Nathan Hunter and Mr. Tony Bennett for proof-reading this manuscript, and Mr. Nakarin Nintawee, Mr. Nattatape Jumpanoi, and Ms. Phitchaporn Sukcharoen for facilitating the work. The authors also would like to express their deep appreciation to the Office of Higher Education Commission (OHEC) for its financial support on this project under Climate Change cluster (CC557A) of the National Research University Program.

4.7 References

[1] M.A. den Hollander, M.Wissink, M. Makkee, J.A. Moulijn, Appl. Catal., A 223 (2002) 85-102.

[2] D.P. Serrano, R. van Grieken, J.A. Melero, A. Garcia, C. Vargas, J. Mol. Catal. A: Chem 318 (2010) 68-74.

[3] K. Yogo, M. Inhara, I. Terasaki, E. Kikuchi, Appl. Catal., B 2 (1993) L1-L5.

[4] P. Borges, R. Ramos Pinto, M.A.N.D.A. Lemos, F. Lemos, J.C. Vedrine, E.G. Derouane, F. Ramoa Ribeiro, Appl. Catal., A 324 (2007) 20-29.

[5] J. Perez-Ramirez, F. Kapteijn, J.C. Groen, A. Domenech, G. Mul, J.A. Moulijn, J. Catal. 214 (2003) 33-45.

[6] H. Feng, C. Li, H. Shan, Appl. Clay Sci. 42 (2009) 439-445.

[7] S. van Donk, A. Broersma, O.L.J. Gijzeman, J.A. van Bokhoven, J.H. Bitter, K.P. de Jong, J. Catal. 204 (2001) 272-280.

[8] Y. Tao, H. Kanoh, Y. Hanzawa, K. Kaneko, Colloids Surf., A 241 (2004) 75-80.

[9] Y. Tao, H. Kanoh, Y. Hanzawa, K. Kaneko, J. Am. Chem. Soc. 125 (2003) 6044-6045.

[10] Y. Tao, Y. Hattori, A. Matumoto, H. Kanoh, K. Kaneko, J. Phys. Chem. B 109 (2005) 194-199.

[11] H. Wang, T.J. Pinnavaia, Angew. Chem., Int. Ed. 45 (2006) 7603-7606.

[12] M. Fujiwara, A. Sakamoto, K. Shiokawa, A.K. Patra, A. Bhaumik, Microporous Mesoporous Mater. 142 (2011) 381-388.

[13] M. Choi, HS. Cho, R. Srivastava, C. Venkatesan, DH. Choi, R. Ryoo, Nat. Mater. 5 (2006) 718-723.

[14] KS. Na, WJ. Park, YB. Seo, R. Ryoo, Chem. Mater. 23 (2011) 1273-1279.

[15] N. Viswanadham, R. Kamble, M. Singh, M. Kumar, G.M. Dhar, Catal. Today 141 (2009) 182-186.

[16] G. Li, E. Kikuchi, M. Matsukata, Microporous Mesoporous Mater. 60 (2003) 225-235.

[17] J. Ozaki, K. Takahashi, M. Sato, A. Oya, Carbon 44 (2006) 1243-1249.

[18] Y. Tao, H. Kanoh, L. Abrams, K. Kaneko, Chem. Rev. 106 (2006) 896-910.

[19] U. Thubsuang, H. Ishida, S. Wongkasemjit, T. Chaisuwan, Carbon (submitted)

[20] X. Ning, H. Ishida, J. Polym. Sci., Part A: Polym. Chem. 32 (1994) 1121-1129.

[21] N.N. Ghosh, B. Kiskan, Y. Yagci, Prog. Polym. Sci. 32 (2007) 1344-1391.

[22] H. Ishida, D.J. Allen, Polymer 37 (1996) 4487-4495.

[23] T. Agag, T. Takeichi, J. Polym. Sci., Part A: Polym. Chem. 45 (2007) 1878-1888.

[24] T. Takeichi, T. Kano, T. Agag, Polymer 46 (2005) 12172-12180.

[25] T. Agag, T. Takeichi, Macromolecules 34 (2001) 7257-7263.

[26] S. Wirasate, S. Dhumrongvaraporn, D.J. Allen, H. Ishida, J. Appl. Polym. Sci. 70 (1998) 1299-1306.

[27] J.A. Macko, H. Ishida, Polymer 42 (2001) 227-240.

[28] J.A. Macko, H. Ishida, Polymer 42 (2001) 6371-6383.

[29] P. Lorjai, T. Chaisuwan, S. Wongkasemjit, J. Sol-Gel Sci. Technol. 52 (2009) 56-64.

[30] P. Katanyoota, T. Chaisuwan, A. Wongchaisuwat, S. Wongkasemjit, Mater. Sci. Eng., B 167 (2010) 36-42.

[31] T. Chaisuwan, T. Komalwanich, S. Luangsukrerk, S. Wongkasemjit, Desalination 256 (2010) 108-114

[32] H. Ishida, US Pat. 5 543 516 (1996).

[33] P. Phiriyawirut, R. Magaraphan, A.M. Jamieson, S. Wongkasemjit, Mater. Sci. Eng., A 361 (2003) 147-154.

[34] H. Robson, Microporous Mesoporous Mater. 22 (1998) 551-666.

[35] B.C. Lippens, J.H. de Boer, J. Catal. 4 (1965) 319-323.

[36] E.P. Barrett, L.G. Joyner, P.P. Halenda, J. Am. Chem. Soc. 73 (1951) 373-380.

[37] L.G. Joyner, E.P. Barrett, R. Skold, J. Am. Chem. Soc. 73 (1951) 3155-3158.

[38] J. Dunkers, H. Ishida, Spectrochim. Acta, Part A 51 (1995) 1061-1074.

[39] N. Job, A. Thery, R. Pirard, J. Marien, L. Kocon, J. Rouzaud, F. Beguin, J. Pirard, Carbon 43 (2005) 2481-2494.

[40] S.J. Gregg, K.S.W. Sing, Adsorption, Surface Area and Porosity, 2nd ed., Academic Press, New York, 1982.

[41] F. Rouquerol, J. Rouquerol, K.S.W. Sing, Adsorption by powders and porous solids, principles, methodology and applications. Academic press, 1999.

[42] F. Guzel, I. Uzun, Turk. J. Chem. 26 (2002) 369-377.

[43] Y. Fang, H. Hu, G. Chen, Microporous Mesoporous Mater. 113 (2008) 481-489.

[44] K. Tang, Y.G. Wang, L.J. Song, L.H. Duan, X.T. Zhang, Z.L. Sun, Mater. Lett. 60 (2006) 2158-2160.

[45] A. Petushkov, S. Yoon, S.C. Larsen, Microporous Mesoporous Mater. 137 (2011) 92-100.

[46] W. Song, R.E. Justice, C.A. Jones, V.H. Grassian, S.C. Larcen, Langmuir 20 (2004) 8301-8306.

[47] W. Song, R.E. Justice, C.A. Jones, V.H. Grassian, S.C. Larcen, Langmuir 20 (2004) 4696-4702.

[48] Y. Cheng, L.J. Wang, J.S. Li, Y.C. Yang, X.Y. Sun, Mater. Lett. 59 (2005) 3427-3430.

[49] G. Coudurier, C. Naccache, J.C. Vedrine, J. Chem. Soc., Chem. Commun. 24 (1982) 1413-1415.

[50] F. Wolf, H. Fuertig, Tonind. Ztg. Keram. Rundsch. 90 (1966) 310.

[51] E.M. Flanigen, in "Zeolite Chemistry and Catalysis", J.A. Rabo, Editor, Am. Chem. Soc. Washington (1976) p. 80.

[52] J. Valyon, J. Mihalyfi, H.K. Beyer, P.A. Jacobs, Proceed. Workshop on Adsorpt. Berlin, DDR (1979) p. 134.

[53] E.M. Glanigen, H. Khatami, H. Szymanski, Adv. Chem. Ser. 101 (1979) 201.

[54] K.-J. Chao, T.C. Tasi, M.-S. Chen, I. Wang, J. Chem. Soc., Faraday Trans. 177 (1981) 547-555.

[55] W. Fan, R. Li, J. Ma, B. Fan, J. Cao, Microporous Mater. 4 (1995) 301-307.

[56] K.F.M.G.J. Scholle, W.S. Veeman, P. Frenken, G.P.M. van der Velden, Appl. Catal. 17 (1985) 233-259.

[57] O.G. Somani, A.L. Choudhari, B.S. Rao, S.P. Mirajkar, Mater. Chem. Phys. 82 (2003) 538-545.

[58] J.C. Jansen, F.J. van der Gaag, H. van Bekkum, Zeolites 4 (1984) 369-372.